Visual Abstract

Influence of internal technological defects on the mechanical properties of structural CFRP

D.S. Lobanov, S.V. Slovikov, E.M. Lunegova
Center of Experimental Mechanics, Perm National Research Polytechnic University, Russia
cem.lobanov@gmail.com, http: //orcid.org/0000-0003-1948-436X
sslovikov@ya.ru, https://orcid.org/ 0000-0003-3884-3882
cem.zubova@mail.ru, https://orcid.org/0000-0001-8829-3546

Abstract. The use of carbon-fiber composite materials (CFRP) in critical cases implies an increase in the resistance to the stability of their mechanical properties. For the purpose of in-depth analysis of defects in the experiments, an integrated approach to mechanical flaw detection and testing of CFRP is used. To determine the parameters of defects in ultrasonic diagnostic sensors and the method of infrared thermography. The main technological defects of structural carbon fiber in samples of the internal "glueline defect", are three geometric shapes (circle, square, rectangle) and a "buckling" inner layer. As a result of flaw detection of individual samples by ultrasonic diagnostics, data were obtained on the shape and size of defects such as "glueline defect" and "buckling". As a result of the study, tensile testing of the samples with and without defects was carried out using the Vic 3D system, the AMSY-6 acoustic emission system, and the FLIR SC7700M thermal imaging system. The tensile strength, elastic modulus, Poisson's ratio, and maximum fracture strains of the studied CFRP without defects and with defects are obtained. The effect of defective zones on the main mechanical parameters is determined. The investigated defects lead to a decrease in strength and elastic characteristics by at least 15% and 5%, respectively.

Keywords. Carbon-fiber composite, Internal technological defects, Tensile, Non-destructive testing, Ultrasonic diagnostics, Infrared thermography, Digital image correlation, Acoustic emission

OPEN ACCESS

Citation: Lobanov, D.S., Slovikov, S.V., Lunegova E.M., Influence of Internal Technological Defects on the Mechanical Properties of Structural CFRP, Frattura ed Integrità Strutturale, 65 (2023) 74-87.

Received: 26.01.2023
Accepted: 28.04.2023
Online first: 01.05.2023
Published: 01.07.2023

Introduction

In many industries, the fields of application of composite materials have been expanding, including in particularly critical areas of structures where the stability of mechanical characteristics is important and significant variations of mechanical properties are not allowed. Often, composites are used where metals were previously used. At the same time, the fact

that the mechanical properties of carbon-fiber composite materials differ widely from those of metals shows increased requirements for the manufacturing process of composite parts minimizing the possibility of technological and operational defects. Studies related to the assessment of the possibility and feasibility of repair and restoration operations for the most dangerous operational defects, as well as their impact on the residual properties of products made of structural composites, are presented in the works [1-2].

During the production of structural carbon-fiber composites and related products, different defects may occur, such as glueline defects, buckling, cracks, delaminations, chips, scratches, porosity, reinforcement scheme irregularities, deviations from the optimal polymerization regime and the nominal density of a binding agent. In their turn, defects affect the mechanical behavior of materials. It is important to understand how the shape, location, and size of defects affect mechanical properties [3–10]. So it follows that the determination of the effect of their shape, size, and location when they occur both in the manufacture of structures and during operation is really relevant.

The papers consider the influence of internal defects, such as fiber microbuckling occurring during compression, on the mechanical properties of fibrous composites [11-12].

When conducting studies of composite materials and structures, it is important for the completeness of the analysis to take a comprehensive, versatile approach based on not one but several measuring and diagnostic systems that both identify technological and operational defects and determine the effect of defects on mechanical properties.

In the presented study, such methods as ultrasonic diagnostics and thermal mapping are used to determine the parameters of defects. When conducting ultrasonic diagnostics of defects during the study, the ultrasonic time-of-flight-diffraction method [13-14] is used.

Thermal analysis is based on the active infrared thermography method [15-17].

To assess the mechanical behavior of materials, a digital optical video system designed to analyze deformation and displacement fields and a system designed to record acoustic emission signals were used.

Optical methods based on the use of digital video systems and the digital image correlation method identify defects, assess their size, and measure the amount of deformation in the observation area [18-21]. During loading, the video system registers the fields of displacements and deformations on the surface of an object with two video cameras using the digital image correlation method as a mathematical apparatus [22].

The acoustic emission method is based on the registration of elastic waves that arise during the deformation of samples. The waves are recorded on the surface of the studied material samples by piezoelectric sensors, after which they are filtered to extract information [21-23]. This method of studying damage processes that occur under the influence of loads is used to identify destruction regularities [26-29].

The relevance of this work is driven by the increasing use of composite materials in critical structures and the corresponding increase in requirements for their mechanical characteristics, as well as the need to assess the impact of both technological and operational defects on changes in mechanical properties and identify the possibility of identifying internal defects in composites.

The novelty of the work to consist in obtaining new experimental data that allow assessing the impact of the presence of internal technological defects of various types and geometry on the mechanical characteristics of the studied composite materials, in performing defect identification based on an integrated approach using a testing system and non-destructive testing systems.

The main purpose of this study is to assess the effect of the most common technological defects on the mechanical properties, deformation regularities, and failure processes of structural carbon-fiber samples with the integrated use of testing and measuring systems and non-destructive testing methods. At this stage of the study, the main tasks were: to establish and work out the most effective diagnostic method and identification modes of the technological defects under study, to determine and analyze the values of the main mechanical characteristics of carbon-fiber samples without internal defects and with technological defects, such as "glueline defects" and "layer buckling".

MATERIAL AND METHODS

Internal "glueline defects" of the layer of different geometric shapes and "buckling" of the inner layer were used as the main technological defects of structural carbon-fiber composites in the samples.

The samples with embedded defect simulators are made of carbon-fiber composites based on equal-strength fabrics by autoclave molding. All the studied samples were cut from one plate. The technological fluoroplastic separating film was used as embedded defects. The defects were located in the middle layer.

The samples were made of structural carbon-fiber composites VKU based on the epoxy VSE1212 binder with a laying scheme $[0/90]_{10}$, with internal technological defects ("glueline defects") implemented by the laid fluoroplastic separating film with geometric shapes: circle ø 20 mm; square 20x20 mm; rectangle 10x40 mm. The internal technological defect "buckling" is represented by a Z-bend of one layer (n5), 25 mm wide (Fig.1). All the defects were laid between the 5th and 6th layers, i.e. in the center of the package.

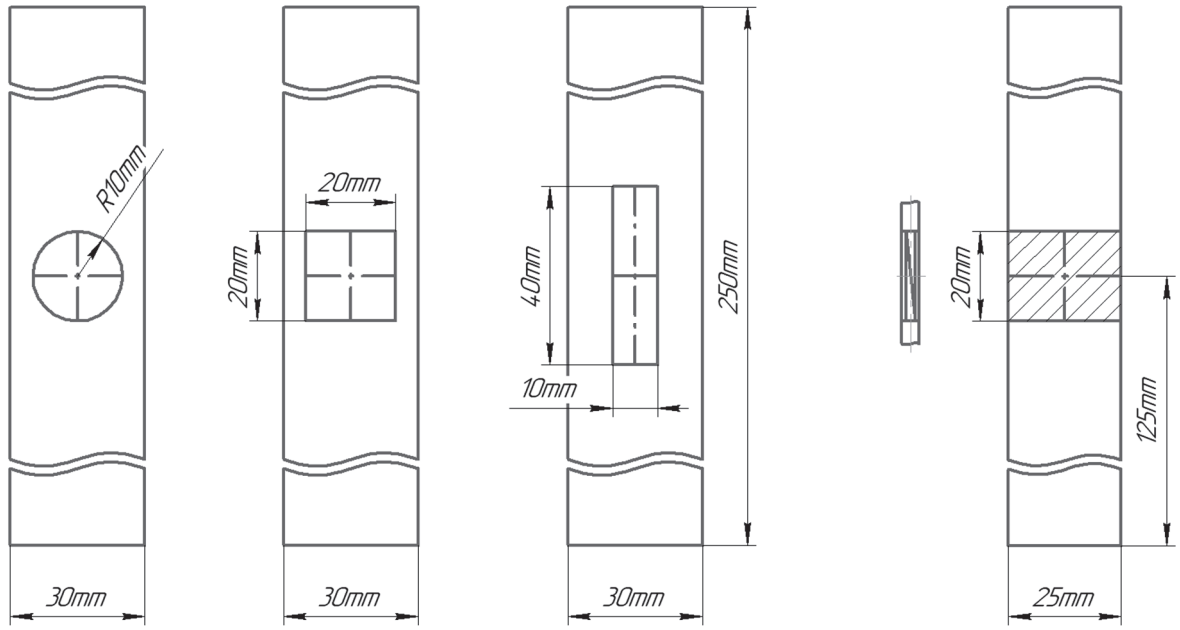

(a) (b)

Figure 1: Scheme of samples with internal "glueline defects" of the layer of different geometric shapes (a) and defect "buckling" of the inner layer (b).

The ultrasonic flaw detection technique was implemented using the Harfang Veo 16-64 flaw detector with a sensor on a phased-array antenna (PAA) (Fig. 2 a, b).
The method of diagnosing defects using a signal sensor based on phased-array antennas ensures the accuracy of determining the detected irregularities. An important feature of PAAs is a non-stationary amplitude-phase distribution that can be controllably changed during research. The digital flaw detector system is based on a 16-bit architecture and provides high-resolution images.

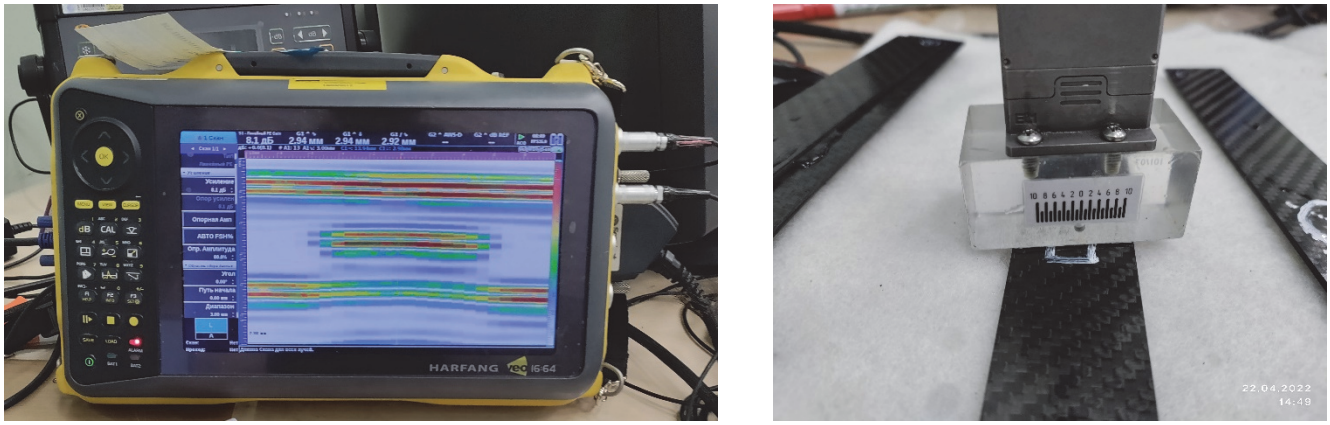

(a) (b)

Figure 2: The ultrasonic flaw detector Harfang Veo 16-64 with a screen showing the "glueline defects" (*a*), and sensor on PAA 32 scanning defect in the sample (*b*)

The infrared thermography technique is implemented using the FLIR SC7700M thermal imaging system (spectral range: 3-5 and 8-12 μm; temperature sensitivity less than 18 mK at +30°C; temperature range from -20 to +3000°C; frame refresh rate 380 Hz; accuracy of at least 1% of absolute temperature). The process of diagnosing defects is shown in Fig. 3.

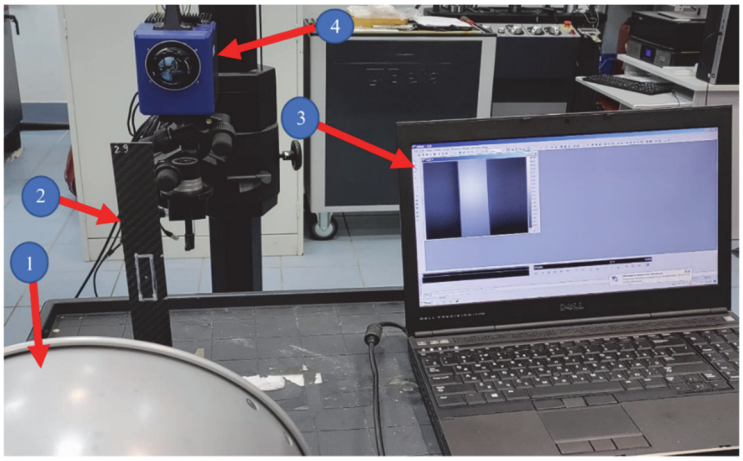

(a)

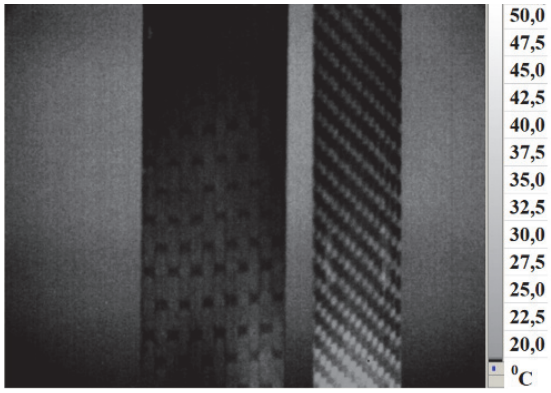

(b)

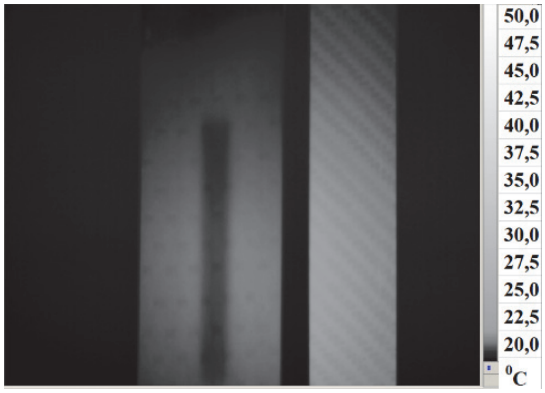

(c)

Figure 3: The infrared thermography: *a* – test scheme (1 infrared source, 2- test sample, 3 - image processing system, 4 - FLIR SC7700M); internal defect monitoring: *b* – samples before heating, *c* – samples after short heating

The thermography technique consisted in short-term heating of the sample surface by an infrared source for 10 seconds to 40-50°C, followed by cooling for 1-2 seconds and registering internal defects manifested due to the temperature field gradient.

An example of registering a 10 mm wide and 90 mm long internal defect laid in 4 layers is shown in Fig. 3. In Fig. 3, b and 3, c, there is a wide sample with a defect on the left and a narrow sample without a defect on the right.

In the application of the technique shown in Fig. 3, the inner cavity of the sample that has an air space does not have time to warm up in a short-term heating mode. When fixing the temperature field with the FLIR SC7700M infrared thermal imaging system, the internal defect looks like a colder area with a temperature of 20.5°C, unlike the rest of the surface which has a temperature of 30.0°C. It should be noted that the samples with "glueline defects" of different geometries and "layer buckling" studied in this project were diagnosed. However, the "buckling" and "glueline defects" were not registered because the laid fluoroplastic film simulating a "glueline defect" had a thermal conductivity similar to that of the material. There was no temperature gradient in the area of the defect. The situation is similar to the identification of the "buckling" defect because in this case it is imitated by the middle layer bend.

The study of the mechanical behavior of carbon-fiber samples under quasi-static tension was carried out on the Instron 5882 universal electromechanical system with a high-precision load sensor in conjunction with an infrared thermography system, the Vic-3D digital optical system designed to analyze displacement fields and the Vallen AMSY-6 system designed to record acoustic emission signals.

The Vic-3D system includes Prosilica 50 mm cameras (resolution 4872 x 3248.16 Mp), the maximum shooting frequency at a maximum resolution of 3 frames per second. In this work, the criterion of the normed sum of squared differences with a zero mean is used since it is the least sensitive to changes in lighting during the test.
During loading, AE signals were recorded by the Vallen AMSY-6 system. The Vallen AMSY-6 acoustic emission system has 8 independent channels designed to collect information.
The work used the AE144A broadband sensor (frequency range 100-500 kHz) and a preamplifier with a gain of 34 dB. The threshold value for recording AE signals was 40 dB.
An energy parameter (E, eu) was used to analyze acoustic emission signals obtained during the mechanical testing of composite materials [30–32].
The AMSY-6 system has the ability to record waveforms of signals, and a special software option analyzes waveforms, spectral characteristics, and spectrum maximum frequency (SMF, kHz) [33-38]. The frequency values were obtained using the Fast Fourier Transform algorithm, and the linear location of acoustic emission sources was implemented.
During the development of research methods, the testing and measuring systems were synchronized to record the load and displacement values and then compare them with additional data. Based on the testing of the techniques, the parameters of post-processing of digital image correlation were selected. The features of the useful signal extraction were worked out, and the most widely used parameters of the acoustic emission signal were considered, which were later used for the visualization, processing, and interpretation of the results obtained during the mechanical loading of composite material samples. The use of linear signal location algorithms was tested. Thermograms in the field of defects in the process of quasi-static stretching of structural carbon-fiber samples were considered.

Results and discussion

As a result of flaw detection of the studied samples by ultrasound diagnostics, data on the shape and size of defects, such as "buckling" and "glueline defects", were obtained.
The "layer buckling" defect is not as obvious as the "glueline defect" and can easily be missed during diagnosis. When a single pulse is passed, a "layer buckling" defect is displayed on the monitor of the ultrasonic flaw detector as a slightly noticeable "step" of the lower reflecting surface. When 2 or more pulses are passed, the signal distortion is summed up and the defect, including the boundaries of the beginning and the end of the defect zone (marked as black ellipses in the figures), is observed more clearly (Fig. 4 a, b). A "glueline defect" is registered by an ultrasonic flaw detector as shown in Fig. 4 c, d, e. (the defect zone is marked by a black dotted line).

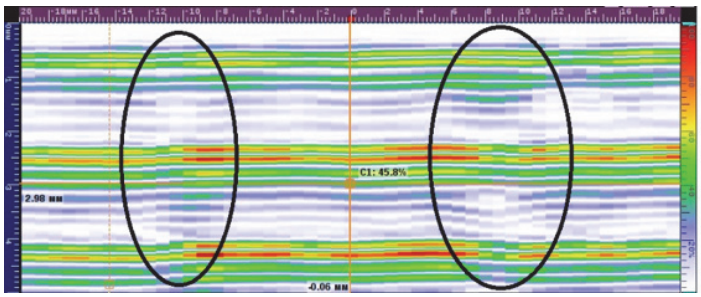

(a)

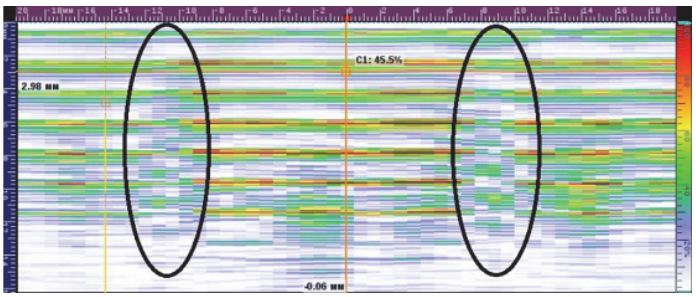

(b)

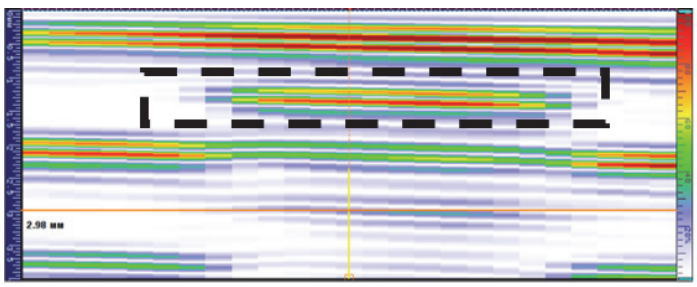

(c)

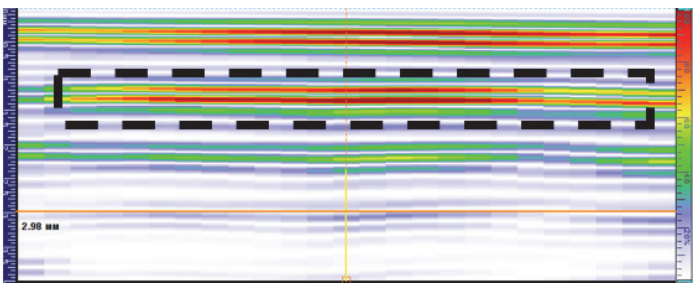

(d)

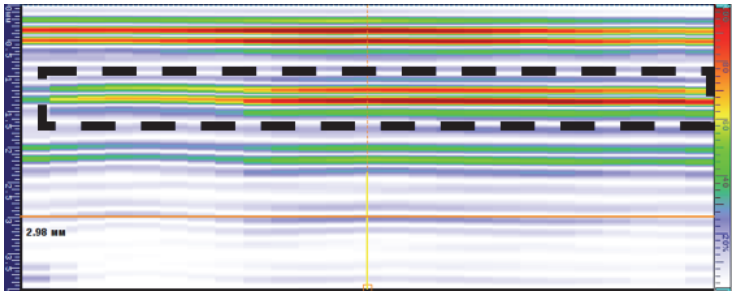

(d)

Figure 4: Description "layer buckling" defect when passing 2 (a) and 6 (b) pulses is displayed on the monitor of the ultrasonic flaw detector; description "glueline defect": (c) –rectangle; (d) – circle; (e) – square (the defect zone is marked by a black dotted line)

Based on the results of tensile tests, diagrams of the loading and deformation of carbon fiber samples were constructed (Fig. 5).

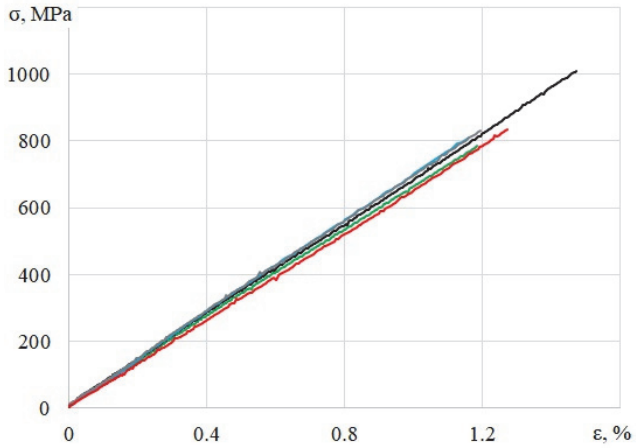

Figure 5: Typical deformation diagrams of carbon fiber samples without defects and with internal defects: without defects – black line; "layer buckling" defect – green line; "glueline defect" circle shape – blue line; "glueline defect" square shape – grey line; "glueline defect" rectangle shape – red line

Fig. 6 shows examples of failure carbon-fiber samples (Reviewer B)with embedded defects pre-painted in a special way for identification using the Vic3D deformation fields. It should be noted that all the tested structural carbon-fiber samples with and without a "glueline defect" were complete failure either (Reviewer B)under the grips or near the grips of the test system. The carbon-fiber samples with a "buckling" defect were failure in the(Reviewer B) working area along the boundaries of the defect.

In the course of comprehensive studies, the data obtained by the AE signal registration analysis system during tensile tests were analyzed. As a result, charts of the distribution of the cumulative energy parameter of AE signals (E, eu) on time (Fig. 7, a) and along the length of the measurement surface (l, m) were constructed (Fig. 8, a-e).

The time distributions of the AE signals cumulative energy (Fig. 7, a) which may reflect the degree of accumulation of defects in the structure of the material during deformation are considered. It was found that these curves have a stage character. At the first stage, which coincides with a gradual increase in the load, the accumulation of defects occurs evenly. At the second stage, at the moment preceding of failure, the rate of accumulation of defects increases, which is reflected in the cumulative energy curve. This staging is typical for all samples. The cumulative energy of AE signals (Fig. 7, a) is maximum for a sample without a defect. For samples with a "glueline defect", the cumulative energy curves are similar and differ in the maximum value of the cumulative energy, where is the maximum value for samples with a «square» defect. And the minimum for a sample with a «rectangle» defect. For example, the graph of cumulative energy with the loading diagrams for a sample without a defect, for a sample with a "glueline defect" a square shape and defect "buckling" were shows (Fig. 7, b-d).

The measurement length was equal to the distance between the AE sensors and was equal to 0.12 m (Fig. 8). (Reviewer B) The boundaries of the embedded defects in the figure are marked by red dotted lines. To determine the location of AE

sources, linear location of signals was used, which is based on determining the speed of the sound wave in the material and the difference time between the signal arrival at sensor 1 and sensor 2. The speed of the sound wave was determined experimentally before testing.

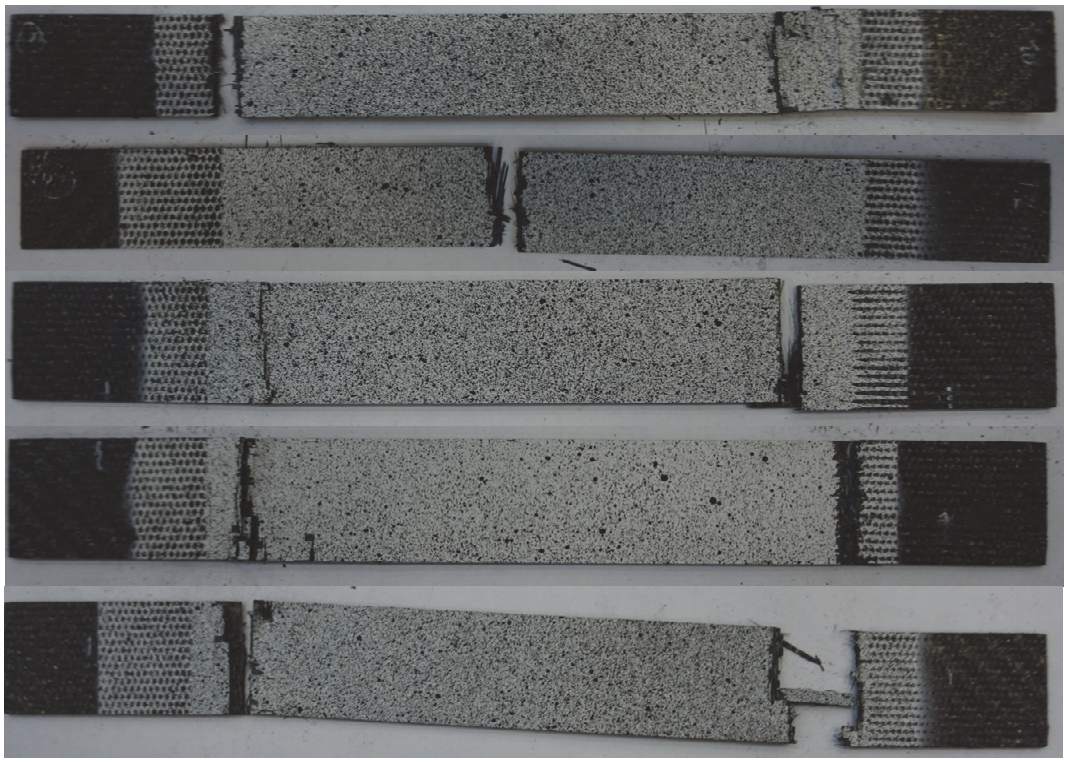

Figure 6: Types of fractures in CFRP specimens: 1 – without defects; 2 – "layer buckling" defect; 3 – "glueline defect", circle shape; 4 – "glueline defect ", square shape; 5 – "glueline defect ", rectangle shape.

Analyzing the graphs, it can be concluded that peak values of the energy parameter were registered at the places of the final failure of the samples. However, as for the samples with embedded defects, an increase in the energy parameter of AE signals was also recorded either at the boundary of the embedded defect or directly in the defect zone.
For the tested samples, the dependences of the distribution of spectral maximum frequency values (F, kHz) of AE signals for the entire loading time were constructed where the vertical axis was the number of registered signals (N, units). Examples of such dependencies are shown in Fig. 9. All the values of the maximum frequency of the spectrum are grouped within 3 ranges: 50-75 kHz (range No. 1), 200-300 kHz (range No. 2), and 310-410 kHz (range No. 3).

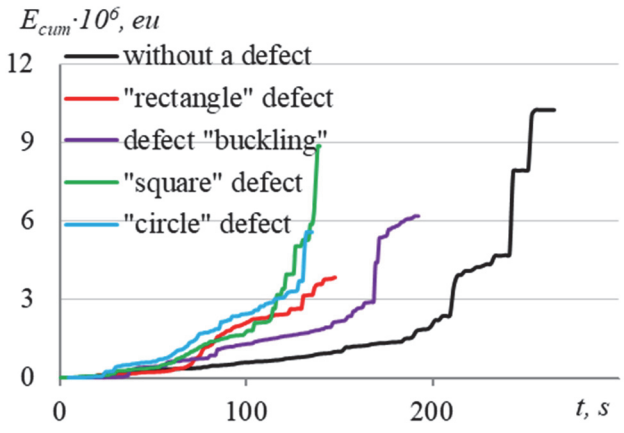

(a)

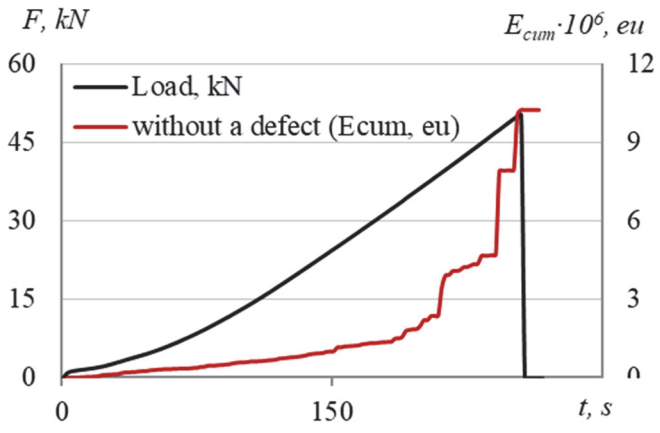

(b)

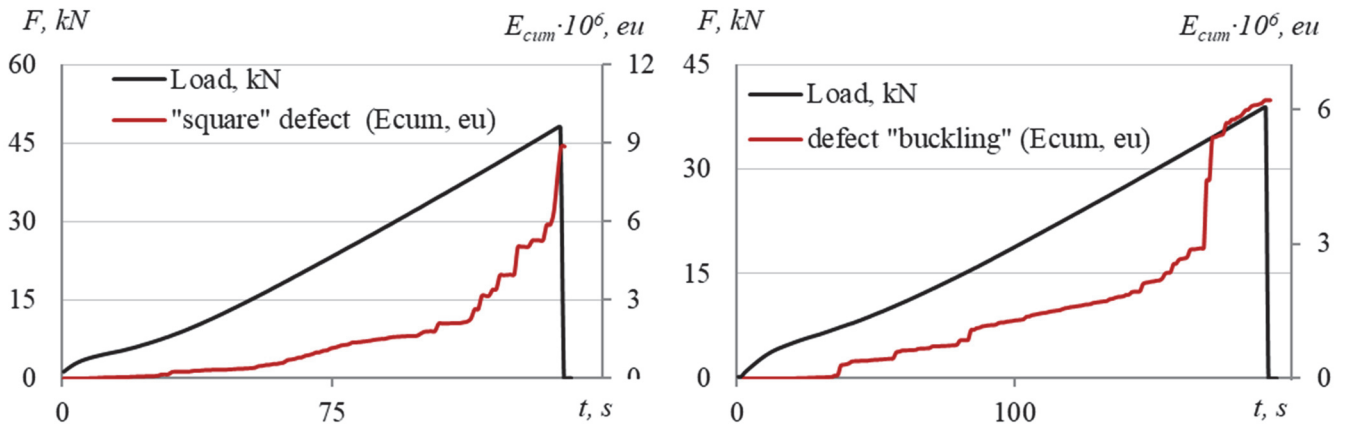

(c) (d)

Figure 7: Distribution AE cumulative energy on time for different samples (a) and distribution of the AE cumulative energy with load diagram for a sample without a defect (b), a sample with a "glueline defect" a square shape (c), a defect "buckling" (d)

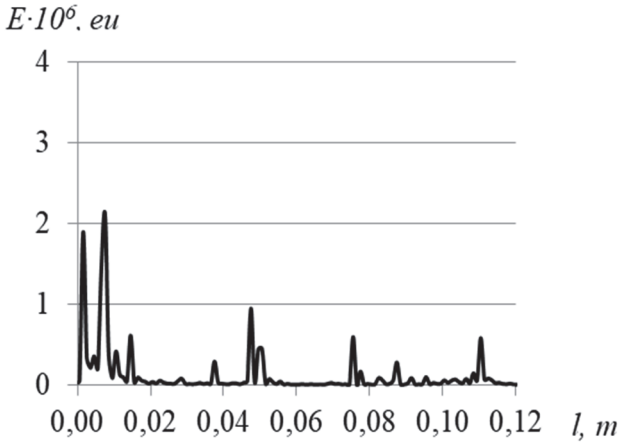

(a)

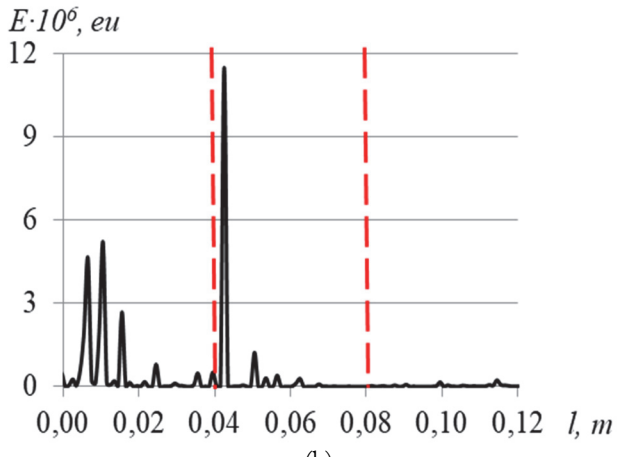

(b)

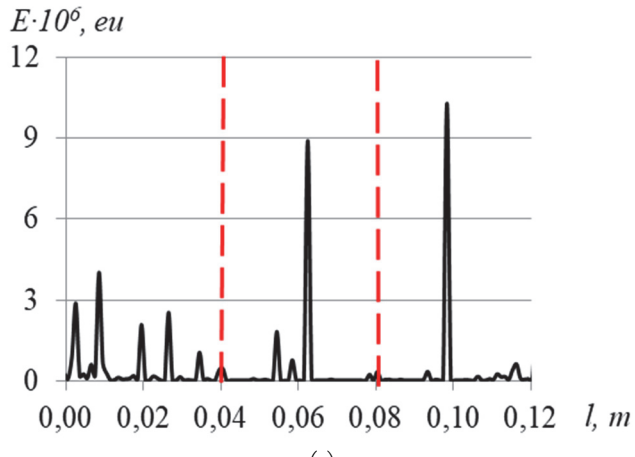

(c)

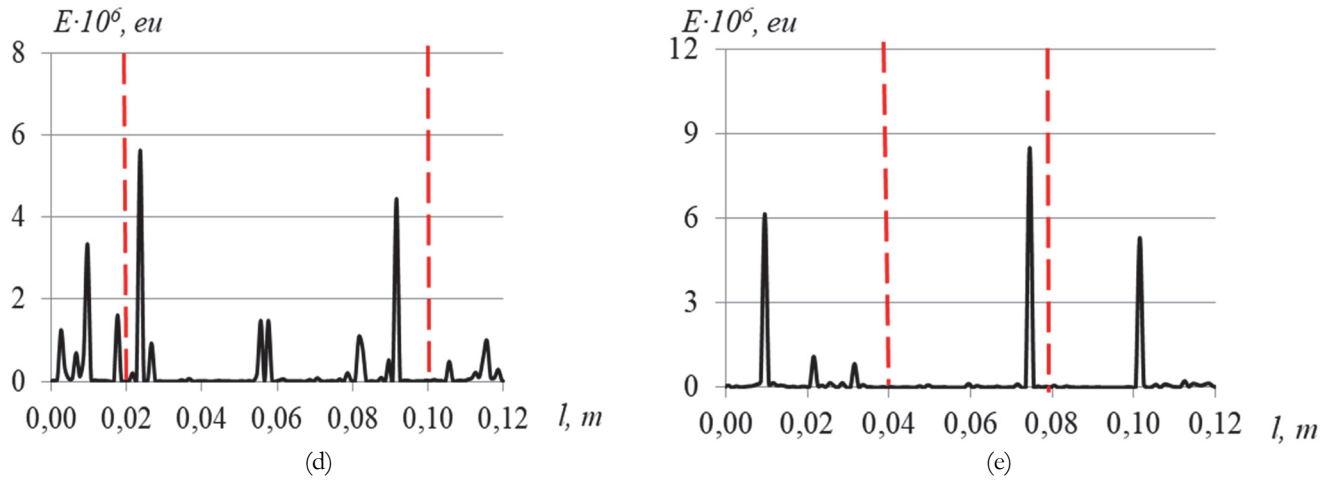

Figure 8: Distribution of the AE energy for a sample without a defect (a), a sample with a "glueline defect", a circle shape (b), a square shape (c), a rectangle shape (d), a defect "buckling" (e)

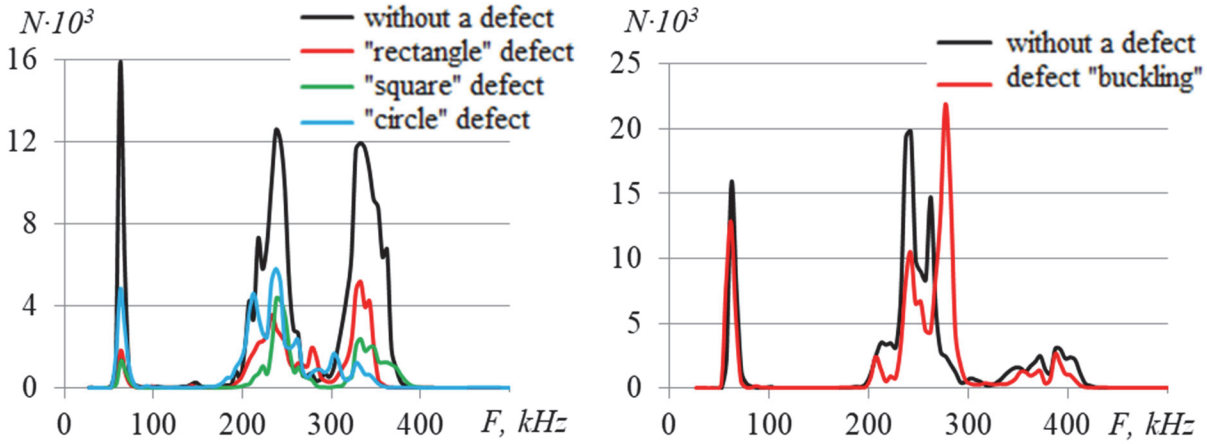

Figure 9: Distribution of AE signals frequency values for samples with various defects

Within all ranges, more signals were registered for the samples without defects than for those with "glueline defects". This may be due to the fact that with the studied geometric sizes of defects, the volume of a binding agent in the sample decreases by a significant amount, which leads to a decrease in the number of registered signals. For example, for the samples with a circular defect, the number of signals decreased by 73±15%, with a square one by 71±15%, and with a rectangular one by 57±10%. At the same time, for the samples with buckling, the number of registered signals is within the statistical range of defect-free samples. Obviously, this phenomenon requires additional research to identify the dependence of changes in the internal structure on the number of signals.

In addition, for the samples with a circular defect in frequency range No. 3, the smallest number of signals among all the samples under consideration was registered. This is due to the round shape of the defect and the absence of stress concentrators, in contrast to the rectangular and square forms of "glueline defects".

When analyzing thermograms of the samples with internal defects, it was found that the "glueline defects" of one layer are not registered by the thermal imaging system during the tensile test until the failure of the sample, regardless of the shape of the defect. For example, the evolutions of the temperature field for the samples without a defect (Fig. 10 a) and for the sample with a "glueline defect", square shape (Fig. 10 b), are given. The internal "buckling" defect of the layer is clearly registered during tensile testing at a load value equal to 0.5-0.7 of the failure load (Fig. 10 c).

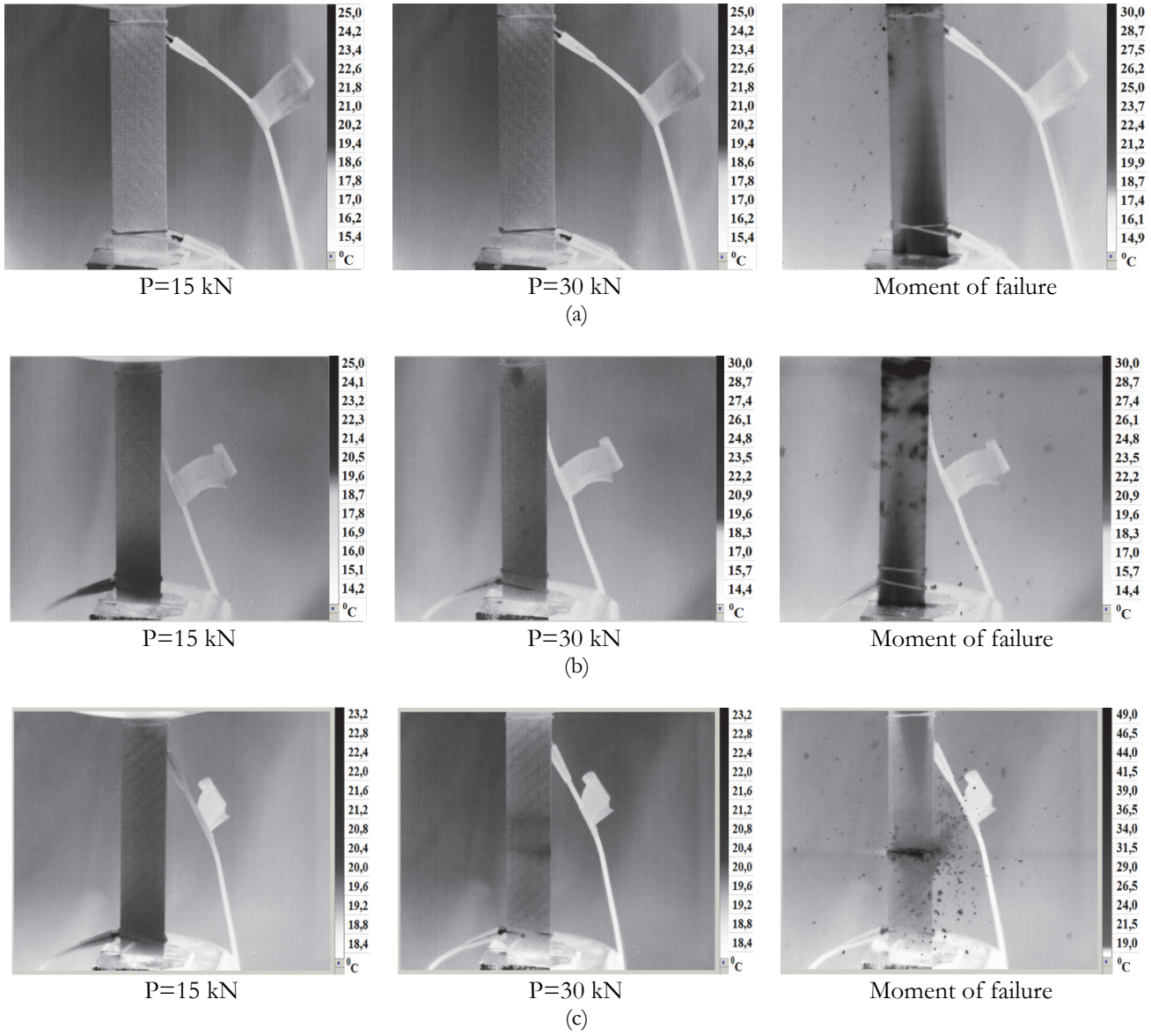

Figure 10: Evolution of the thermogram: *a* - without a defect, *b* - "glueline defect", square shape, *c* - the internal "buckling" defect of the inner layer .

Based on the test results, the main mechanical properties (tensile strength, modulus of elasticity, maximum deformations during failure) were obtained and presented in Tab. 1. 95% confidence intervals were obtained using the Student's method.

No	Type of defect	Elastic modulus, GPa	Tensile strength, MPa	Max load, kN
1	"layer buckling" defect	64.7±2.0	830±49	39.5±2.4
2	"glueline defect", circle shape	68.2±0.4	815±40	45.4±2.1
3	"glueline defect", square shape	67.3±2.0	892±92	48.9±4.8
4	"glueline defect", rectangle shape	65.1±0.8	863±60	47.1±3.1
5	without a defect	66.1±1.0	954±52	50.3±1.3

Table 1: Tensile properties of CFRP specimens.

According to the tensile tests of carbon-fiber samples, the effect of the type ("glueline defect ", "buckling") and geometry (circle, square, rectangle) of the defect was assessed. According to the results of tensile tests, it was found that the "glueline defect" of any geometry in one layer does not affect the change in the mechanical properties of structural carbon-fiber

composites during tensile. The "buckling" defect leads to a decrease in strength characteristics by at least 15%, and modulus of elasticity – by 5%.

As a result of the analysis, deformation fields were obtained for different components during loading. An example of deformation fields under the same loads for the samples with an internal "glueline defect" at P≈ (0.75 - 0.85) P max = 40 kN, and for the samples with an internal "buckling" defect at P≈ (0.75 -0.85) P max = 30 kN are shown in Fig. 11, where yellow lines highlight the places of defective areas.

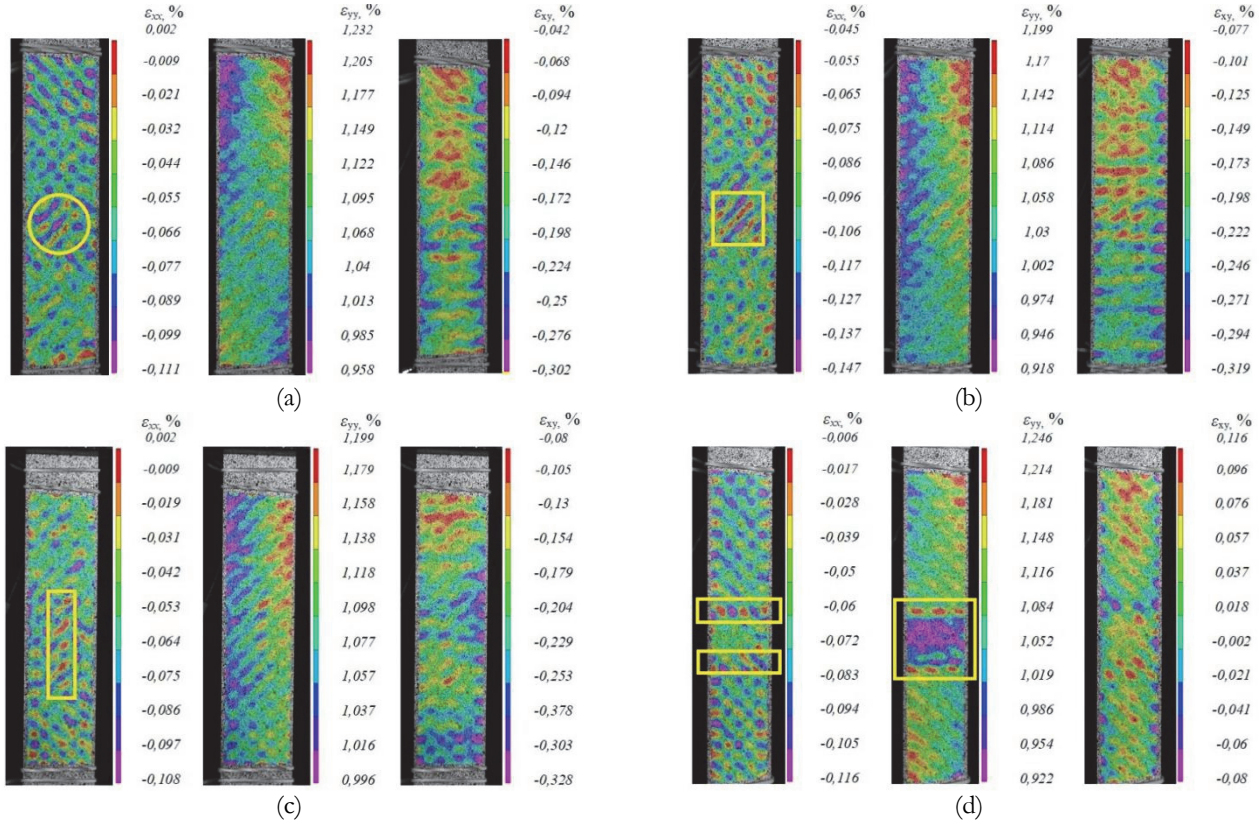

Figure 11: Fields of deformations ε_{xx}, ε_{yy}, ε_{xy} on the surface of CFRP samples with internal "glueline defect", circle shape (*a*), square shape (*b*), rectangle shape (*c*) and the "layer buckling" defect (*d*).

As a result of the analysis, the presence of deformation localization places was noted, which makes it possible to determine the location of the "glueline defect" of each geometry (Fig. 11 *a, b,* c), as well as the boundaries of the "buckling" defect of the inner layer (Fig. 11 *d*). The "glueline defect" is viewed mainly in the field of transverse deformations (the ε_{xx} component). The "buckling" defect is clearly registered by the fields of longitudinal and transverse deformation (the ε_{xx} and ε_{yy} components).

Conclusions

As a result of flaw detection of the samples under study by ultrasound diagnostics, the data on the shape and size of defects, such as "glueline" and "buckling" defects, were obtained. The "layer buckling" defect is not as obvious as the "glueline defect" and can easily be missed during diagnosis.

As a result of the study, tensile testing of the samples with and without defects was carried out using the Vic 3D system, the AMSY-6 acoustic emission system, and the FLIR SC7700M thermal imaging system.

Based on the tensile test results, the diagrams of loading and deformation of carbon-fiber samples were constructed. The basic mechanical properties (tensile strength, modulus of elasticity and maximum deformations during failure) were obtained. The data obtained by the AE signal registration analysis system were analyzed.

When analyzing thermograms of the samples with internal defects, it was found that the "glueline defects" are not registered by the thermal imaging system during the tensile test until the failure of the sample, regardless of the shape of the defect.
According to the tensile test results, it was found that the "glueline defect" of any geometry in one layer does not affect the change in the mechanical properties of structural carbon-fiber composites during tensile. The "buckling" defect leads to a decrease in strength characteristics by at least 15%, and modulus of elasticity – by 5%.
As a result of the analysis, the deformation fields were obtained for different components during loading and the presence of localization places was noted, which makes it possible to determine the location of a "glueline defect" of each geometry, as well as the boundaries of a "buckling" defect of the inner layer.

Acknowledgements

This work was carried out with the support of the Russian Science Foundation (Project No 21-79-10205, https://rscf.ru/project/21-79-10205/, accessed on 13 December 2022) at the Perm National Research Polytechnic University.

References

[1] Anoshkin, A.N., Vil'deman, V.E., Lobanov, D.S., Chikhachev, A.I. (2014). Evaluation of Repair Efficiency in Structures Made of Fibrous Polymer Composite Materials, Mech Compos Mater, 50(3), pp. 311–316. DOI: 10.1007/s11029-014-9416-0.

[2] Anoshkin, A.N., Zuiko, V.Y., Tashkinov, M.A., Silberschmidt, V.V. (2015). Repair of damage in aircraft composite sound-absorbing panels, Composite Structures, 120, pp. 153–166. DOI: 10.1016/j.compstruct.2014.10.001.

[3] Cantwell, W.J., Morton, J. (1992). The significance of damage and defects and their detection in composite materials: A review, The Journal of Strain Analysis for Engineering Design, 27(1), pp. 29–42. DOI: 10.1243/03093247V271029.

[4] Armstrong, K.B. (2005). Care and Repair of Advanced Composites, 2nd edition, Warrendale, Pa, SAE International.

[5] Senthil, K., Arockiarajan, A., Palaninathan, R., Santhosh, B., Usha, K.M. (2013). Defects in composite structures: Its effects and prediction methods – A comprehensive review, Composite Structures, 106, pp. 139–149. DOI: 10.1016/j.compstruct.2013.06.008.

[6] Lobanov, D.S., Wildemann, V.E., Spaskova, E.M., Chikhachev, A.I., (2015). Experimental investigation of defects influence on composites sandwich panels strength using digital image correlation and infrared thermography methods, PNRPU Mechanics Bulletin, (4), pp. 159–170. DOI: 10.15593/perm.mech/2015.4.10.

[7] Tashkinov, M.A. (2017). Modelling of fracture processes in laminate composite plates with embedded delamination, Frattura Ed Integrità Strutturale, 11(39), pp. 248–262. DOI: 10.3221/IGF-ESIS.39.23.

[8] Xie, N., Smith, R.A., Mukhopadhyay, S., Hallett, S.R. (2018). A numerical study on the influence of composite wrinkle defect geometry on compressive strength, Materials & Design, 140, pp. 7–20. DOI: 10.1016/j.matdes.2017.11.034.

[9] Wildemann, V.E., Tretyakova, T.V., Strungar, E.M., Tretyakov, M.P. (2018). Deformation and failure of carbon fiber composite specimens with embedded defects during tension-torsion test, Frattura Ed Integrità Strutturale, 12(46), pp. 295–305. DOI: 10.3221/IGF-ESIS.46.27.

[10] Lobanov, D.S., Strungar, E.M., Zubova, E.M., Wildemann, V.E. (2019). Studying the Development of a Technological Defect in Complex Stressed Construction CFRP Using Digital Image Correlation and Acoustic Emission Methods, Russ J Nondestruct Test, 55(9), pp. 631–638. DOI: 10.1134/S1061830919090031.

[11] Soutis C., Curtis P.T. (2000) A method for predicting the fracture toughness of CFRP laminates failing by fibre microbuckling, Composites Part A: Applied Science and Manufacturing, 31(7), pp. 733-740. DOI: 10.1016/S1359-835X(00)00003-8

[12] Greco F., Lonetti P., Luciano R., Nevone Blasi P., Pranno A. (2018) Nonlinear effects in fracture induced failure of compressively loaded fiber reinforced composites, Composite Structures, 189, 688-699. DOI: 10.1016/j.compstruct.2018.01.014

[13] Garnier, C., Pastor, M.-L., Eyma, F., Lorrain, B. (2011). The detection of aeronautical defects in situ on composite structures using Non Destructive Testing, Composite Structures, 93(5), pp. 1328–1336. DOI: 10.1016/j.compstruct.2010.10.017.

[14] Meo, M., Polimeno, U., Zumpano, G. (2008). Detecting Damage in Composite Material Using Nonlinear Elastic Wave Spectroscopy Methods, Appl Compos Mater, 15(3), pp. 115–126. DOI: 10.1007/s10443-008-9061-7.

[15] Vavilov, V.P., Nesteruk, D.A., Shiryaev, V.V., Ivanov, A.I., Swiderski, W. (2010). Thermal (infrared) tomography: Terminology, principal procedures, and application to nondestructive testing of composite materials, Russ J Nondestruct Test, 46(3), pp. 151–161. DOI: 10.1134/S1061830910030010.
[16] Vavilov, V., Burleigh, D. (2019). Infrared thermography and thermal nondestructive testing, Switzerland, Springer Cham. DOI: 10.1007/978-3-030-48002-8.
[17] Chulkov, A., Vavilov, V., Nesteruk, D., Burleigh, D., Moskovchenko, A., (2023). A method and apparatus for characterizing defects in large flat composite structures by Line Scan Thermography and neural network techniques, Frattura ed Integrità Strutturale, 63, 110-121.
[18] Anoshkin, A.N., Voronkov, A.A., Kosheleva, N.A., Matveenko, V.P., Serovaev, G.S., Spaskova, E.M., Shardakov, I.N., Shipunov, G.S. (2016). Measurement of inhomogeneous strain fields by fiber optic sensors embedded in a polymer composite material, Mech. Solids, 51(5), pp. 542–549. DOI: 10.3103/S0025654416050058.
[19] Matveenko, V.P., Shardakov, I.N., Voronkov, A.A., Kosheleva, N.A, Lobanov, D.S., Serovaev, G.S., Spaskova, E.M., Shipunov, G.S. (2017). Measurement of strains by optical fiber Bragg grating sensors embedded into polymer composite material, Structural Control and Health Monitoring, 25, p. e2118. DOI: 10.1002/stc.2118.
[20] Fedorov, A.Y., Kosheleva, N.A., Matveenko, V.P., Serovaev, G.S. (2020). Strain measurement and stress analysis in the vicinity of a fiber Bragg grating sensor embedded in a composite material, Composite Structures, 239, p. 111844. DOI: 10.1016/j.compstruct.2019.111844.
[21] Strungar, E., Lobanov, D., Wildemann, V. (2021). Evaluation of the Sensitivity of Various Reinforcement Patterns for Structural Carbon Fibers to Open Holes during Tensile Tests, Polymers, 13(24), p. 4287. DOI: 10.3390/polym13244287.
[22] Sutton, M.A., Orteu, J.-J., Schreier, H. (2009). Image Correlation for Shape, Motion and Deformation Measurements, Boston, MA, Springer US, DOI: 10.1007/978-0-387-78747-3.
[23] de Souza, L.R., Marques, A.T., d'Almeida, J.R.M. (2017). Effects of aging on water and lubricating oil on the creep behavior of a GFRP matrix composite, Composite Structures, 168, pp. 285–291. DOI: 10.1016/j.compstruct.2017.02.041.
[24] Lobanov, D.S., Zubova, E.M. (2019). Research of temperature aging effects on mechanical behaviour and properties of composite material by tensile tests with used system of registration acoustic emission signal, Procedia Structural Integrity, 18, pp. 347–352. DOI: 10.1016/j.prostr.2019.08.174.
[25] Lobanov, D., Zubova, E. (2020). Temperature aging effects on mechanical behavior of structural GFRP on interlaminar shear tests, IOP Conference Series: Materials Science and Engineering, 747, p. 012119. DOI: 10.1088/1757-899X/747/1/012119.
[26] Sause, M.G.R., Gribov, A., Unwin, A.R., Horn, S. (2012). Pattern recognition approach to identify natural clusters of acoustic emission signals, Pattern Recognition Letters, 33(1), pp. 17–23. DOI: 10.1016/j.patrec.2011.09.018.
[27] Al-Jumaili, S.K., Holford, K.M., Eaton, M., McCrory, J.P., Pearson, M.R., Pullin, R. (2015). Classification of acoustic emission data from buckling test of carbon fibre panel using unsupervised clustering techniques, Structural Health Monitoring, 14, pp. 241–251.
[28] Panteleev, I., Naimark, O. (2015). Identification of fracture mechanisms of fiberglass laminate based on the acoustic emission data, AIP Conference Proceedings, 1683(1), p. 020178. DOI: 10.1063/1.4932868.
[29] Carvelli, V., D'Ettorre, A., Lomov, S.V. (2017). Acoustic emission and damage mode correlation in textile reinforced PPS composites, Composite Structures, 163, pp. 399–409. DOI: 10.1016/j.compstruct.2016.12.012.
[30] Kharrat, M., Ramasso, E., Placet, V., Boubakar, M.L. (2016). A signal processing approach for enhanced Acoustic Emission data analysis in high activity systems: Application to organic matrix composites, Mechanical Systems and Signal Processing, 70–71, pp. 1038–1055. DOI: 10.1016/j.ymssp.2015.08.028.
[31] Ivanov, S.G., Beyens, D., Gorbatikh, L., Lomov, S.V. (2017). Damage development in woven carbon fibre thermoplastic laminates with PPS and PEEK matrices: A comparative study, Journal of Composite Materials, 51, pp. 637–647.
[32] Zubova, E.M., Lobanov, D.S., Strungar, E.M., Wildemann, V.E., Lyamin, Y.B. (2019). Application of the Acoustic Emission Technique to Studying the Damage Accumulation in a Functional Ceramic Coating, PNRPU Mechanics Bulletin, (1), pp. 39–49. DOI: 10.15593/perm.mech/2019.1.04.
[33] Pollock, A. (1989). Acoustic Emission Inspection, Metals Handbook. Ninth Edition ASM International, (17), pp. 278–294.
[34] AMSY-6 Handbook. Developed and manufactured by Vallen Systeme GmbH. (2012).
[35] Arumugam, V., Saravanakumar, K., Santulli, C. (2018). Damage characterization of stiffened glass-epoxy laminates under tensile loading with acoustic emission monitoring, Composites Part B: Engineering, 147, pp. 22–32.

DOI: 10.1016/j.compositesb.2018.04.031.
[36] Barile, C., Casavola, C., Pappalettera, G., Vimalathithan, P.K. (2019). Damage characterization in composite materials using acoustic emission signal-based and parameter-based data, Composites Part B: Engineering, 178, p. 107469. DOI: 10.1016/j.compositesb.2019.107469.
[37] Dia, A., Dieng, L., Gaillet, L., Gning, P.B. (2019). Damage detection of a hybrid composite laminate aluminum/glass under quasi-static and fatigue loadings by acoustic emission technique, Heliyon, 5(3), p. e01414. DOI: 10.1016/j.heliyon.2019.e01414.
[38] Savino, R., Criscuolo, L., Di Martino, G.D., Mungiguerra, S. (2018). Aero-thermo-chemical characterization of ultra-high-temperature ceramics for aerospace applications, Journal of the European Ceramic Society, 38(8), pp. 2937–2953. DOI: 10.1016/j.jeurceramsoc.2017.12.043